Preprints.org

Article

Conversion of Hard to Soft Magnetic Ferrite Nanowires by Paramagnetic Shielding

Xian-Lin Zeng [*] , Indujan Sivanesarajah , Uwe Hartmann

Article

Conversion of Hard to Soft Magnetic Ferrite Nanowires by Paramagnetic Shielding

Xian-Lin Zeng *, Indujan Sivanesarajah and Uwe Hartmann

Institute of Experimental Physics, Saarland University, D-66123 Saarbrücken, Germany
* Correspondence: mophiese@gmail.com

Abstract: In this study, we investigate the magnetization behavior of coaxial nanowires fabricated through the sol-gel electrospinning method. Our analysis uncovers a significant reduction in coercivity for $CoFe_2O_4$ nanowires when $BaTiO_3$ is used as the shell material, effectively transforming them from hard to soft magnetic. This intriguing behavior is attributed to the magnetization reversal effect at the interface between ferromagnetic and paramagnetic regions, and it is also observed in $NiFe_2O_4$ and Fe_2O_3 nanowires. Surprisingly, introducing a $GdBa_2Cu_3O_7$ shell induces a similar effect. Additionally, we employ magnetic impedance measurements on the coaxial nanowires, unveiling their potential for magnetic field sensing applications.

Keywords: electrospinning; core-shell structure; coaxial nanowire; ferrite; magnetic reversal

1. Introduction

As a class of materials renowned for their unique blend of physical properties, chemical stability, and cost-effectiveness, ferrites have gained increasing popularity across a wide range of applications [4]. Among these, $CoFe_2O_4$ stands out with its mixed cubic spinel structure (Fd3m space group), occupying a distinctive position between soft and hard magnetic ferrites and often classified as a semi-hard material. The emergence of nanotechnology has further enriched the properties of ferrites, leading to the application of nanocrystalline $CoFe_2O_4$ in magnetic recording, magnetic fluids, magnetic drug delivery, sensors, electrical devices, optoelectronics, and photocatalytic activities, among others [5–8]. Researchers have achieved high coercivity and saturation magnetization in nanocrystalline $CoFe_2O_4$ by introducing doping with various transition metals into its host spinel ferrite structure [9–15]. The $CoFe_2O_4$ anisotropic particles with size between 5.1 and 12.5 nm have been reported showcasing superparamagnetic behavior [16]. Such nano-sized ferrites have been found utility in magnetic data storage, magnetic imaging, and microwave devices [17,18].

In the realm of multiferroic systems, the $CoFe_2O_4$@$BaTiO_3$ system has garnered significant attention, attracting fundamental research and applications in novel memory devices and magnetic field sensors [19–23]. Coercivity in CoFe2O4@BaTiO3 materials is influenced by the size of $CoFe_2O_4$ particles and the magnetic dipolar interactions between them. For instance, when the particles are within the superparamagnetic size limit and fully isolated by BaTiO3, a low coercivity of 15 Oe can be achieved [24]. On the other hand, core-shell $CoFe_2O_4$@$BaTiO_3$ particles, with sizes between 40 and 60 nm, exhibit higher coercivity (264 Oe), while the core-shell CoFe2O4@BaTiO3 nanotubes (diameter around 100 nm) exhibit comparable coercivity to pure $CoFe_2O_4$ nanotubes, reaching 901 Oe.

In this study, we present intriguing results obtained from coaxial electrospun $CoFe_2O_4$@$BaTiO_3$ nanowires with an average diameter over 200 nm, revealing unexpected soft magnetism compared to the relatively hard magnetic behavior observed in pure $CoFe_2O_4$ nanowires. This behavior cannot be solely attributed to superparamagnetic effects as observed in isolated $CoFe_2O_4$ particles. To gain insight into this magnetism variation, we investigate the influence of core and shell materials in coaxial nanowires. Additionally, magnetic impedance measurements are applied to the aligned coaxial nanowires, demonstrating their potential application in magnetic field sensing. These findings shed light on the intriguing properties of coaxial $CoFe_2O_4$@$BaTiO_3$ nanowires and hold promise for future magnetic sensing applications.

2. Materials and Methods

2.1. Preparation of Coaxial Nanowires

The fabrication of all the nanowires is achieved through the sol-gel electrospinning method, employing commercially available chemicals from Alfa Aesar GmbH. All the chemicals are above analytical grade. To prepare the $CoFe_2O_4$ precursor, cobalt acetate ($Co(Ac)_2*4H_2O$) and iron nitrite ($Fe(NO)_3*9H_2O$) are weighted in the molar ratio Co : Fe = 1 : 2 and dissolved in deionized water, the polymer polyvinylpyrrolidone (PVP) (MW 1,300,00) is then mixed with solution as to increase the viscosity of the precursor, preparing for the following electrospinning process. Table 1 listed the precursor recipes of all the required chemical phases in this work.

Table 1. List of precursor recipes for the required chemical phase in this work.

Phase	Chemicals			Molar Ratio			Solvent
$CoFe_2O_4$	$Co(Ac)_2*4H_2O$	$Fe(NO)_3*9H_2O$		1	2		water
$NiFe_2O_4$	$Ni(Ac)_2*4H_2O$	$Fe(NO)_3*9H_2O$		1	2		water
Fe_2O_3		$Fe(NO)_3*9H_2O$		-			water
$BaTiO_3$	$Ba(Ac)_2$	$Ti(C_16H_{36}O_4)$		1	1		Propionic acid
$GdBa_2Cu_3O_7$	$Gd(Ac)_3*xH_2O$	$Ba(Ac)_2$	$Cu(Ac)_2$	1	2	3	Propionic acid

To fabricate coaxial nanowires, we utilize a specially designed coaxial nozzle (Figure 1B) integrated into the electrospinning setup (Figure 1C). The coaxial nozzle comprises two nozzles with different diameters. The inner nozzle is centered using a rubber holder, while the outer nozzle is equipped with a branch connector to enable connection to the secondary syringe.

During the electrospinning process, as depicted in Figure 1A, the core precursor and shell precursor are housed in separate syringes, both driven by the same microspeed boost pump. As the two different precursors emerge, they form a core-shell liquid sphere. Upon applying high voltage to the outer nozzle, the core-shell sphere becomes ionized and morphs into a coaxial jet under the influence of the electric field force between the high voltage nozzle and the grounding collector. Consequently, the coaxial fibers are drawn and collected on the collector. Subsequent thermal treatment at 650 ^oC yields the desired phase configuration in the coaxial nanowires.
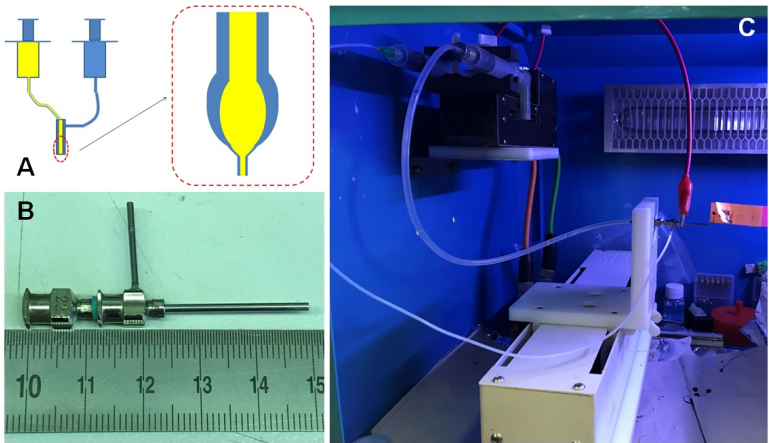

Figure 1. A. Scheme of coaxial electrospinning process; B. Image of the coaxial electrospinning nozzle; C. Image of the coaxial electrospinning setup.

2.2. Sample Preparation for the Magnetic Impedance Measurement

Typically, the collected electrospun nanowires are randomly distributed. To conduct magnetic impedance measurements on these nanowires, it becomes necessary to align them. This alignment can be accomplished through the electric field distribution on the collection area of the electrospinning setup (as illustrated in Figure 2A). Subsequently, the aligned nanowires can be readily 'picked up' using a silicon wafer (as demonstrated in Figure 2C).
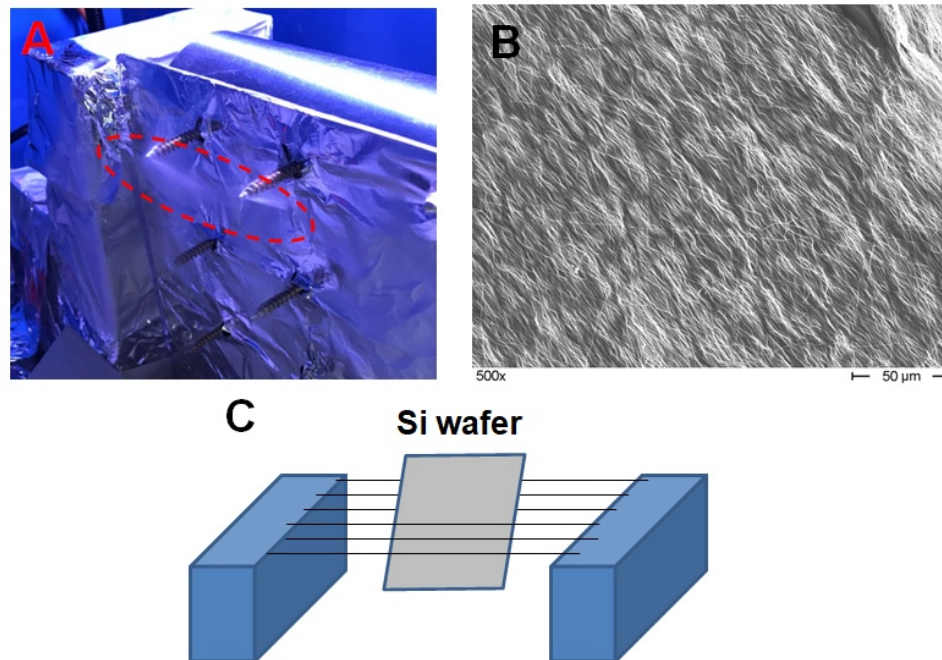

Figure 2. A. collection setup for aligned nanowires; B. SEM image of aligned nanowires; C. approach of transporting aligned nanowires to a silicon wafer.

In the subsequent stage, we employ Laser lithography (μPG 101 from Heidelberg Instruments) to write an electric connection pattern on the aligned nanowires. Due to the specific orientation of the nanowires, applying the electric pattern precisely on the area where the nanowires are located allows for straightforward identification of the electric pattern covering them. Subsequently, the nanowires undergo a sputtering process in the magnetic sputter instrument, resulting in a 300 nm copper layer being deposited on top of the nanowires, as depicted in Figure 3. With the copper pattern now covering both ends of the nanowire, a solid electric connection between the electric pattern and the nanowire can be expected.

To conduct magnetic impedance measurements on the nanowires, we utilize a vector analyzer (Rohde und Schwarz ZNL-3) featuring a three-pin connection. According to this setup, the upper part of the electric pattern serves as the ground connection, while the bottom part is designated for the source connection.
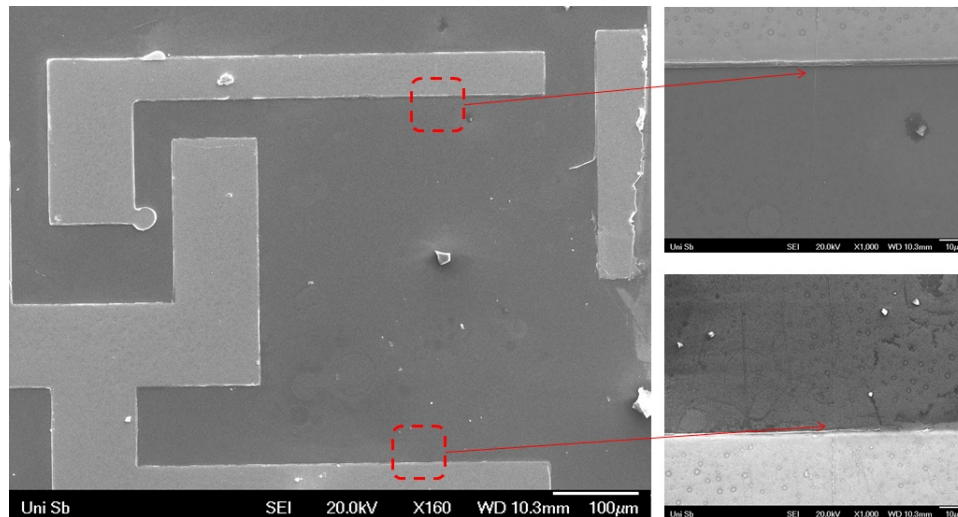
Figure 3. SEM of the nanowire with electric pattern for magnetic impedance measurement

2.3. Remaining Experimental Details

The chemical phases of the samples were identified using a high-resolution automated RINT2200 X-ray powder diffractometer with Cu-K$_{\alpha}$ radiation (40 kV, 40 mA). The microstructure characterization involved SEM imaging with a Hitachi S800 at 10 kV and TEM analysis using JEOL JSM-7000 F (200 kV, LaB$_6$ cathode), which also included EDAX element analysis. For magnetic property characterization, the samples were examined via PPMS (Quantum Design 6000).

3. Results and Discussion

3.1. Microstructure of the Samples

To evaluate the suitability of the coaxial nozzle for coaxial nanowire fabrication, we initially utilized BaTiO$_3$ precursor as the shell material, while the core precursor consisted of a mixture of PVP and propionic acid. As illustrated in Figure 4A, the organic component underwent decomposition and evaporation during the thermal treatment, resulting in the formation of BaTiO$_3$ nanotubes with the desired perfect shape. In comparison, the CoFe$_2$O$_4$@BaTiO$_3$ coaxial nanowires exhibit a completely solid appearance as shown in Figure 4B. Both the BaTiO$_3$ nanotubes and CoFe$_2$O$_4$@BaTiO$_3$ coaxial nanowires have average diameters of approximately 200 nm. The average grain size of the coaxial nanowires ranges from 20 nm to 50 nm. These results confirm the absence of the superparamagnetic effect in these nanowires, as the grain size exceeds the promising limit for such effect.
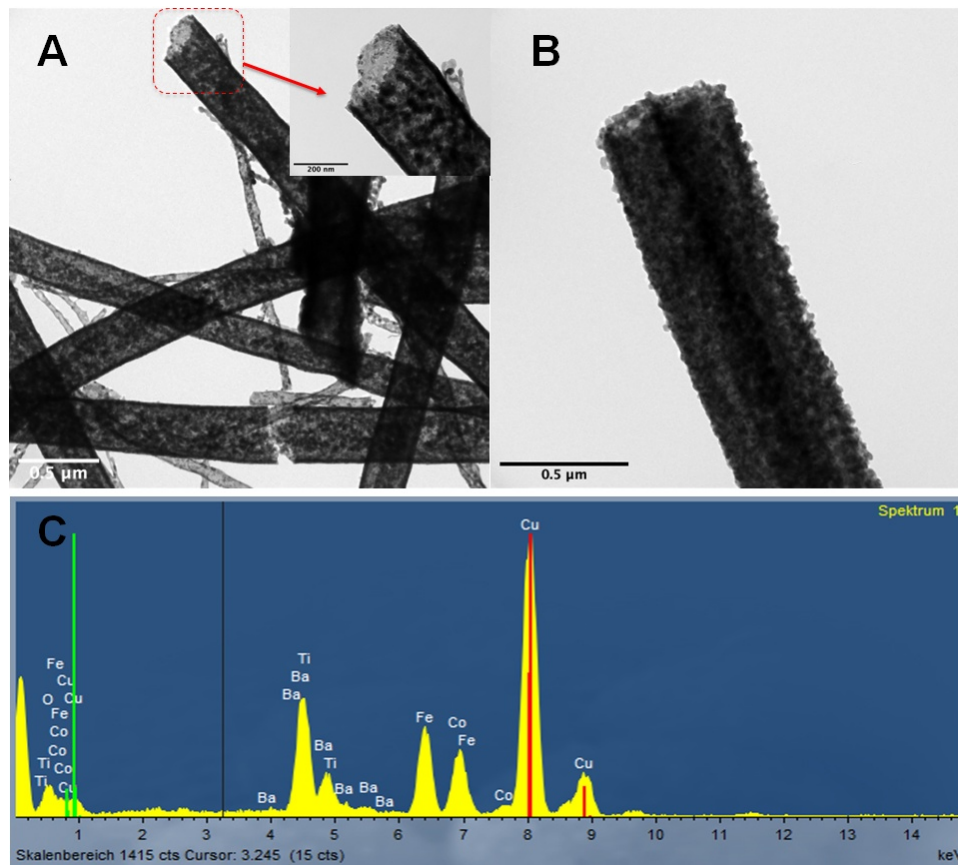
Figure 4. A. TEM image of the $BaTiO_3$ nanotubes; B. TEM image of the $CoFe_2O_4@BaTiO_3$ coaxial nanowire; C. EDAX analysis of the $CoFe_2O_4@BaTiO_3$ coaxial nanowire

3.2. Phase Analysis of the Coaxial Nanowires

Figure 4C displays the EDAX analysis results of the coaxial nanowires, indicating an atomic ratio of Co : Fe : Ba : Ti = 16.23 : 30.35 : 28.02 : 25.40. This confirms the presence of both $CoFe_2O_4$ and $BaTiO_3$ phases in the coaxial nanowires, with an approximate molar ratio of 1 : 2. Furthermore, Figure 5 presents the XRD pattern of the coaxial nanowires, providing additional evidence for the existence of both $CoFe_2O_4$ and $BaTiO_3$ phases. The XRD refinement analysis reveals a mass ratio between the two phases as 22.52 : 77.48, which, when converted to a molar ratio, becomes 22.41 : 77.59. The higher ratio of $BaTiO_3$ phase can be attributed to its shell configuration on the nanowires, as the XRD diffraction signals mainly originate from the surface. Considering this aspect, the phase ratio estimated from EDAX analysis is deemed more reliable.
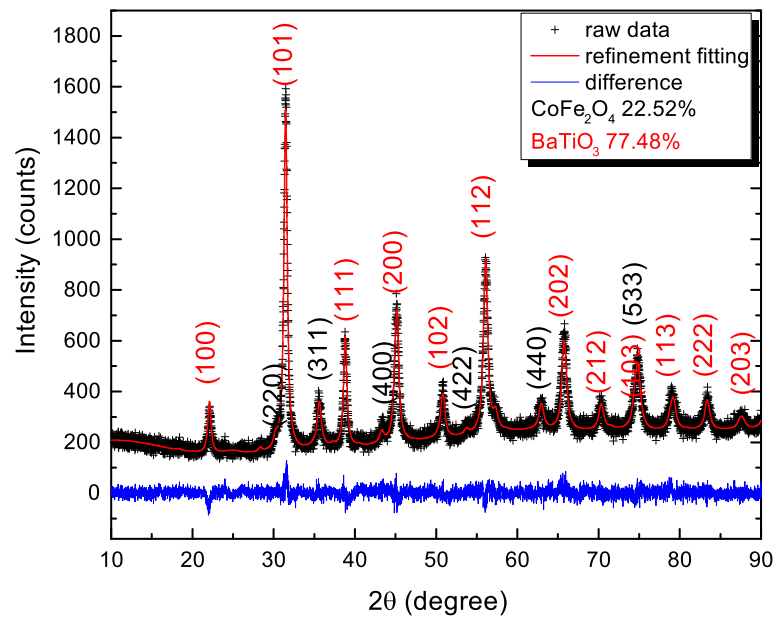
Figure 5. XRD of the $CoFe_2O_4@BaTiO_3$ coaxial nanowires with XRD refinement and phase analysis

3.3. Magnetic Properties of the Samples

Figure 6A illustrates the $M(H)$ magnetization loop of the pure $CoFe_2O_4$ nanowires at 295 K, exhibiting a coercivity (H_C) of 468 Oe, with the saturation field at 4700 Oe. When compared to the electrospun $CoFe_2O_4$ nanowires from another study [25], the coercivity of these nanowires is relatively lower, possibly due to lattice defects induced during the thermal treatment. Nevertheless, these nanowires still fall into the category of 'hard magnetic' materials. Surprisingly, a striking transformation occurs when a paramagnetic shell of $BaTiO_3$ is introduced. As depicted in Figure 6C, the coercivity of the $CoFe_2O_4@BaTiO_3$ coaxial nanowires reduces significantly to 5 Oe, and the saturation field is now at 495 Oe. In essence, the incorporation of a $BaTiO_3$ shell causes a shift from hard magnetic to soft magnetic behavior in the $CoFe_2O_4$ nanowires.

As previously discussed, the reduction of coercivity in these coaxial nanowires cannot be explained solely by the superparamagnetic effect. Instead, the $CoFe_2O_4@BaTiO_3$ coaxial nanowire can be seen as a multilayer system, with paramagnetic (PM) layers ($BaTiO_3$) at the top and bottom, and a ferromagnetic (FM) layer ($CoFe_2O_4$) at the center. When an external magnetic field is applied to the system, the magnetizations of the different layers align parallel to the field direction. However, when the external magnetic field opposes the magnetization of the FM region, the PM region develops a magnetic moment proportional to its susceptibility. These induced moments decay exponentially with distance away from the interfaces [26]. In this configuration, the magnetization of the FM region becomes antiparallel to the induced PM magnetization. Such a setup is energetically unfavorable, leading to an increase in the interlayer exchange energy. Interestingly, this energy facilitates the magnetization reversal process of the FM region, favoring the parallel alignment of the magnetizations of the PM and FM regions. Consequently, a reduction in the coercivity field is observed. Based on this analysis, it becomes evident that the interface energy plays a crucial role in assisting the magnetization reversal process of the FM region, especially when the magnetization of the FM region and the external magnetic field are opposite to each other.

For comparison, we attempted to exchange the core material to $BaTiO_3$ while the shell material became $CoFe_2O_4$, resulting in a coercivity (H_C) of 79 Oe for the new coaxial nanowires as shown in Figure 6D. The reduction of coercivity still persists, although it is not as pronounced as in the previous configuration. This is attributed to the system transforming into an FM / PM / FM multilayer setup, where the magnetization reversal process is constrained by the presence of the shell FM layer.
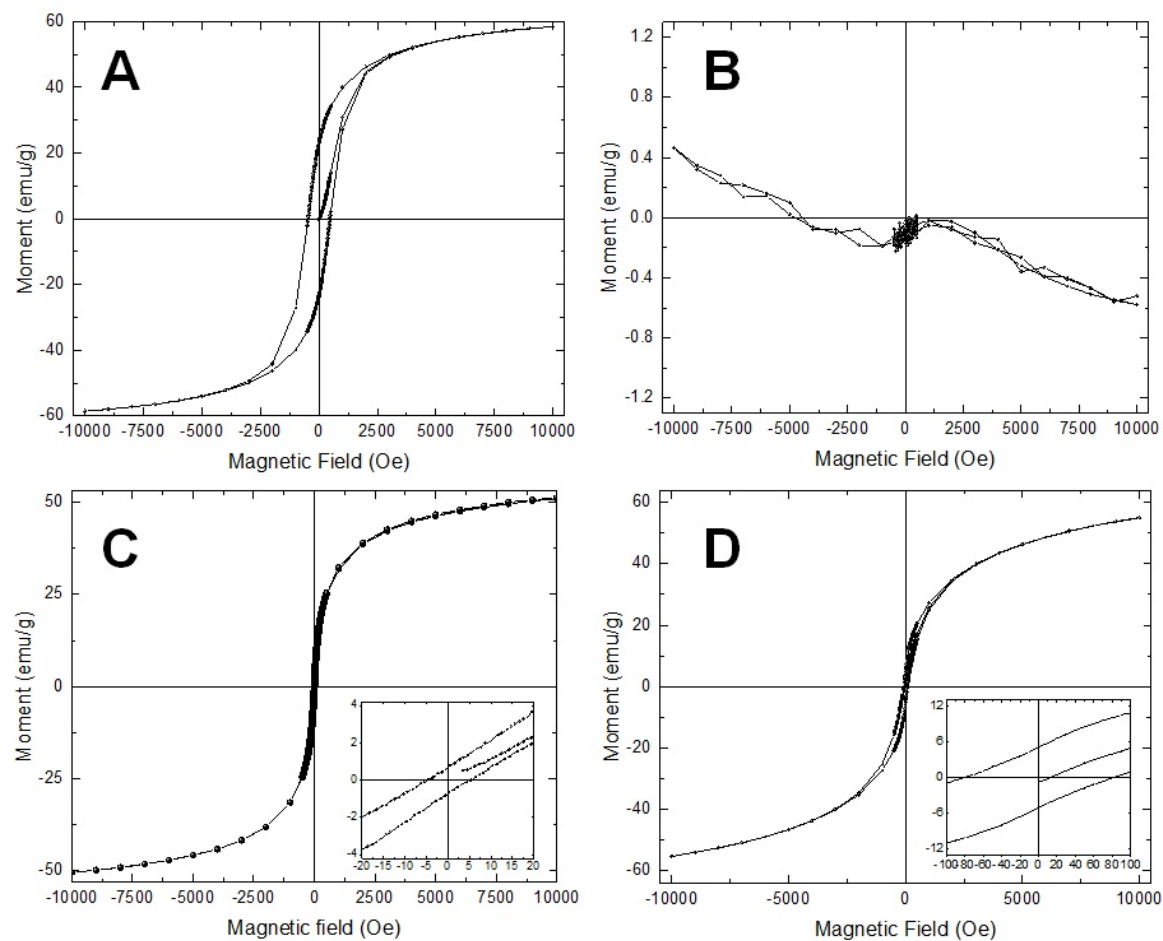
Figure 6. M(H) magnetization of nanowires at 295 K: A. $CoFe_2O_4$ nanowires; B. $BaTiO_3$ nanotubes; C. $CoFe_2O_4@BaTiO_3$ coaxial nanowires; D. $BaTiO_3@CoFe_2O_4$ coaxial nanowires

In our further investigation, we sought to understand the magnetization behavior of the coaxial nanowires as we varied the phase ratio. Achieving this was simple by decreasing the $BaTiO_3$ concentration in the corresponding precursor. Figure 7 presents the magnetization results of the coaxial nanowires with different phase ratios. When $CoFe_2O_4$: $BaTiO_3$ = 1 : 1 (Figure 7A), the coercivity of the samples remained small at H_C = 6.7 Oe. However, this value increased to 146.3 Oe when the molar ratio of the $BaTiO_3$ phase was doubled. This observation indicates that as the ratio of the $BaTiO_3$ phase decreases, the magnetization reversal effect from the FM / PM interface weakens progressively. This explains why in the work of Raidongia et al., the coaxial nanowires synthesized via hydrothermal treatment exhibited a coercivity comparable to pure $CoFe_2O_4$ nanowires [21]. The low ratio of $BaTiO_3$ phase led to the absence of the magnetization reversal effect.
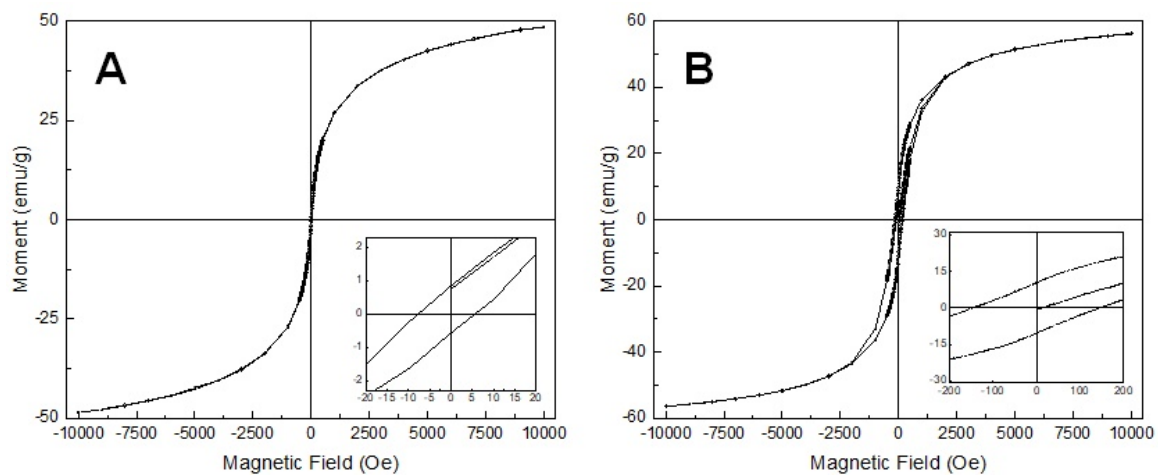
Figure 7. M(H) magnetization of $CoFe_2O_4$@$BaTiO_3$ coaxial nanowires with different phase ratio: A. $CoFe_2O_4$: $BaTiO_3$ = 1 : 1; B. $CoFe_2O_4$: $BaTiO_3$ = 2 : 1

In the subsequent stage, we aimed to investigate whether the magnetization reversal effect was specific to $CoFe_2O_4$@$BaTiO_3$ coaxial nanowires or not. To explore this, we replaced the core material of $CoFe_2O_4$ with $NiFe_2O_4$ and Fe_2O_3, and then measured the magnetization behavior of the newly formed coaxial nanowires. As depicted in Figure 8A–D, the $NiFe_2O_4$ nanowires exhibited a coercivity of 210 Oe. However, upon adding a $BaTiO_3$ shell, the coercivity reduced significantly to 9.5 Oe. A similar trend was observed with the Fe_2O_3 nanowires, where the coercivity decreased from 133 Oe to 8.5 Oe after incorporating a $BaTiO_3$ shell.

Through occasional attempts, we made an intriguing discovery that $BaTiO_3$ is not the sole material capable of serving as the paramagnetic (PM) layer for magnetization reversal in the coaxial nanowire system. As demonstrated in Figure 8E, a noticeable reduction in coercivity also occurs with the $GdBa_2Cu_3O_7$ shell (H_C = 48 Oe). At 5 K, the hysteresis loop of the $CoFe_2O_4$@$GdBa_2Cu_3O_7$ coaxial nanowires displays a ferromagnetic loop. However, it is evident that the shape of the hysteresis loop is influenced by the superconducting component, as shown in the inset of Figure 8F.
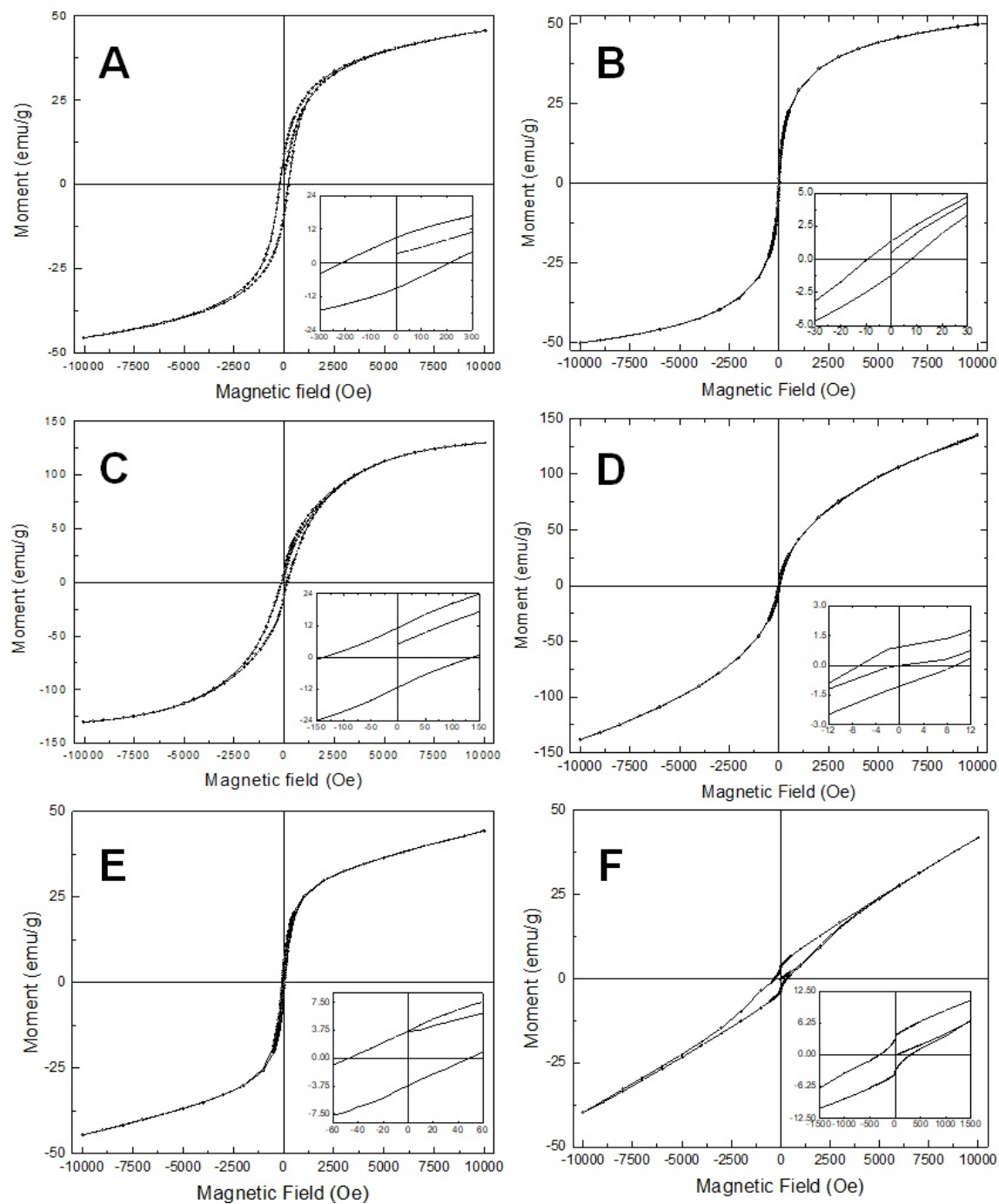
Figure 8. A-D: M(H) magnetization of ferrite nanowires and their corresponding coaxial nanowires: A. NiFe$_2$O$_4$ nanowire, B. NiFe$_2$O$_4$@BaTiO$_3$ coaxial nanowires, C. Fe$_2$O$_3$ nanowires, D. Fe$_2$O$_3$@BaTiO$_3$ coaxial nanowires; E-F: M(H) magnetization of CoFe$_2$O$_4$@GdBa$_2$Cu$_3$O$_7$ coaxial nanowires: E: 295 K; F: 5 K.

3.4. Magnetic Impedance Measurement of the Coaixal Nanowires

Figure 9 illustrates the magnetic impedance results of the CoFe$_2$O$_4$@BaTiO$_3$ coaxial nanowires across the frequency range from 10 MHz to 3 GHz. At 20 MHz, a single peak emerges with a maximum at 57.5 Oe, and the ratio increases with frequency up to 370% at 3 GHz. Another peak appears at 40 MHz, reaching a maximum at -53.8 Oe, and its ratio increases with frequency up to 77% at 3 GHz.

The small misalignment of the nanowire (not precisely perpendicular to the connected pattern) causes an angle between the current and external field, resulting in the occurrence of a second peak.

Additionally, the written contact pads may inadvertently catch more than one nanowire, leading to a mixed signal. Moreover, since the wires are not field treated, the magnetization becomes randomly oriented.

In conclusion, the nanowires exhibit a high GMI ratio that can be utilized for magnetic field sensing. However, the preferred configuration is the double peak, as the linear range between those two peaks can be employed. To achieve this, the following options can be utilized: 1. Preparing the nanowires with an external field perpendicular to the length dimension during heat treatment; 2. Inducing helical anisotropy through joule heating.
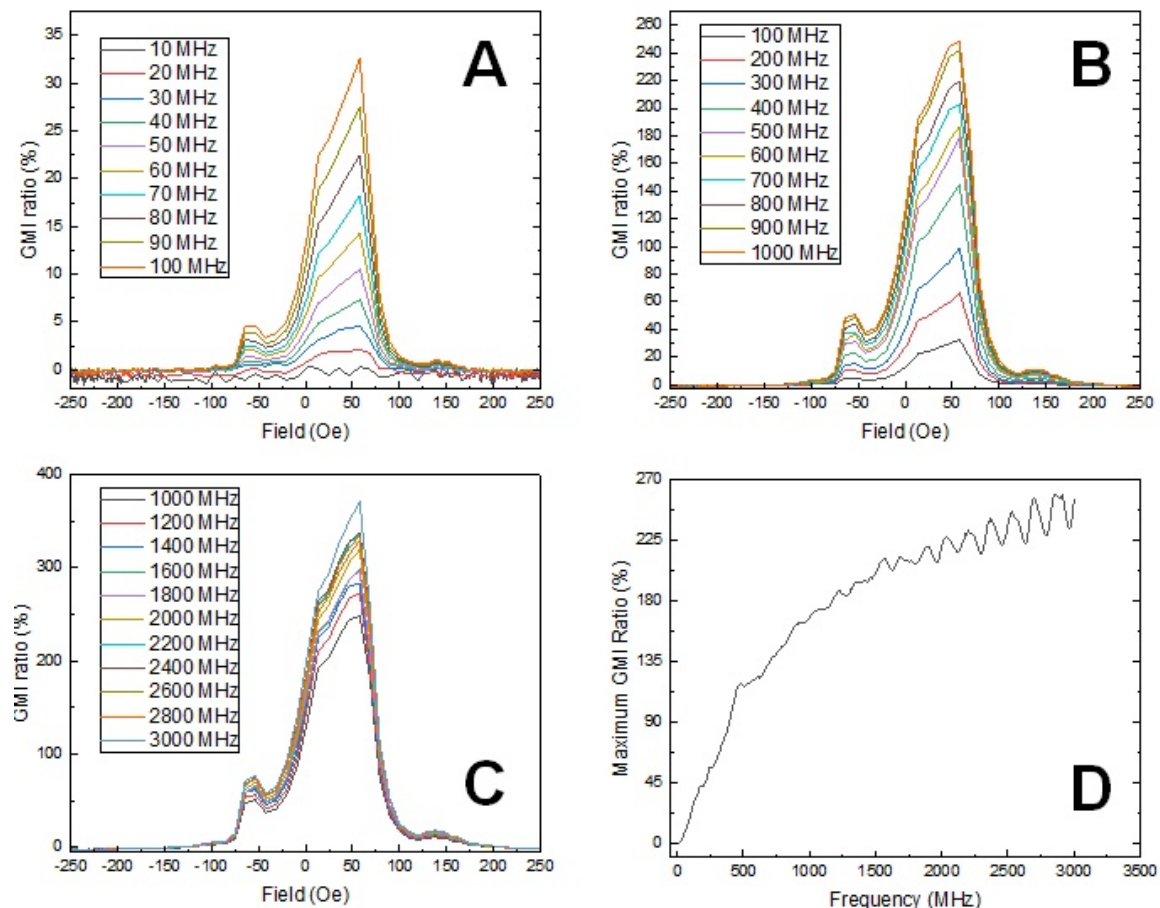

Figure 9. A-C: Magnetic impedance measurement of the $CoFe_2O_4@BaTiO_3$ coaxial nanowires: A. 10 MHz - 100 MHz, B. 100 MHz - 1 GHz, C. 1 GHz - 3 GHz; D. Maximum GMI ratio dependance on frequency.

4. Conclusions

In this study, we investigated the magnetization behavior and properties of $CoFe_2O_4@BaTiO_3$ coaxial nanowires, along with their variations when different core materials were used. Our findings revealed a remarkable reduction in coercivity when a $BaTiO_3$ shell was introduced to the $CoFe_2O_4$ core, leading to a shift from hard magnetic to soft magnetic behavior. This intriguing magnetization reversal effect was also observed when $GdBa_2Cu_3O_7$ was used as the shell material. Additionally, we explored the impact of different phase ratios on the coercivity, further validating the significance of the PM layer in the nanowires' magnetic behavior.

Moreover, we discovered that the misalignment of the nanowire affected the observed magnetic impedance behavior, leading to the emergence of multiple peaks. We suggested possible approaches, such as external field treatment or inducing helical anisotropy, to optimize the configuration and utilize the double peak for magnetic field sensing.

Throughout the investigation, our research sheds light on the versatile characteristics of coaxial nanowires and their promising applications, especially in the realm of magnetic field sensing.

Author Contributions: Conceptualization, Xian-Lin Zeng; methodology, Xian-Lin Zeng; validation, Uwe Hartmann; investigation, Xian-Lin Zeng, Indujan Sivanesarajah; resources, Uwe Hartmann; data curation, Xian-Lin Zeng; writing–original draft preparation, Xian-Lin Zeng; supervision, Uwe Hartmann. All authors have read and agreed to the published version of the manuscript.

Conflicts of Interest: The authors declare no conflict of interest.

Sample Availability: Samples of the compounds ...... are available from the authors.

References

1. Jin, S.; Tiefel, T.H.; McCormack, M.; Fastnacht, R. A.; Ramesh, R.; Chen, L. H. Thousandfold change in resistivity in magnetoresistive La-Ca-Mn-O films. *Science* **1994**, *264*, 413-415.
2. Rodriguez, L.M.; Attfield, J.P. Cation disorder and size effects in magnetoresistive manganese oxide perovskites. *Phys. Rev. B* **1996**, *54*, R15622-R15625.
3. Ramirez, A.P. Colossal magnetoresistance. *J. Phys.: Condens. Matter* **1997**, *9*, 8171-8199.
4. Mathew D. S., Juang R.-S. An overview of the structure and magnetism of spinel ferrite nanoparticles and their synthesis in microemulsions *Chem. Eng. J.* **2007**, *129*, 51-65.
5. Naseri M.G., Saion E.B., Ahangar H.A., Shaari A.H., Hashim M. Simple Synthesis and Characterization of Cobalt Ferrite Nanoparticles by a Thermal Treatment Method *J. Nanomater* **2010**, *2010*, 907686.
6. Patil D.R., Chougule B.K. Effect of copper substitution on electrical and magnetic properties of NiFe2O4 ferrite *Mater. Chem. Phys.* **2009**, *117*, 35-40.
7. Fan H.M., Yi J.B., Yang Y., Kho K.W., Tan H.R., Shen Z.X., Ding J., Sun X.W., Olivo M.C., Feng Y.P. Single-Crystalline MFe2O4 Nanotubes/Nanorings Synthesized by Thermal Transformation Process for Biological Applications *ACS Nano* **2009**, *3*, 2798-2808.
8. Laokul P., Arthan S., Maensiri S., Swatsitang E. Magnetic and Optical Properties of CoFe2O4 Nanoparticles Synthesized by Reverse Micelle Microemulsion Method *J. Supercond. Nov. Magn.* **2015**, *28*, 2483-2489.
9. Koseoglu Y., Alan F., Tan M., Yilgin R., Ozturk M. Low temperature hydrothermal synthesis and characterization of Mn doped cobalt ferrite nanoparticles *Ceram. Int.* **2012**, *38*, 3625-3634.
10. Bhame S.D., Joy P.A. Tuning of the magnetostrictive properties of CoFe2O4 by Mn substitution for Co *J. Appl. Phys.* **2006**, *100*, 113911.
11. Koseoglu Y., Baykal A., Gozuak F., Kavas H. Structural and magnetic properties of $Co_xZn_{1-x}Fe_2O_4$ nanocrystals synthesized by microwave method *Polyhedron* **2009**, *28*, 2887-2892.
12. Kasapoglu N., Birsoz B., Baykal A., Koseoglu Y., Toprak M.S. Synthesis and magnetic properties of octahedral ferrite $Ni_xCo_{1-x}Fe_2O_4$ nanocrystals *Cent. Eur. J. Chem.* **2007**, *5(2)*, 570-580.
13. Moradmard H., Farjami Shayesteh S., Tohidi P., Abbas Z., Khaleghi M. Structural, magnetic and dielectric properties of magnesium doped nickel ferrite nanoparticles *J. Alloys Compd.* **2015**, *650*, 116-122.
14. Zhou B., Zhang Y.W., Liao C.S., Yan C.H. Magnetism and phase transition for $CoFe_{2-x}Mn_xO_4$ nanocrystalline thin films and powders *J. Magn. Magn. Mater.* **2002**, *247*, 70-76.
15. Chae K.P., Lee J.-G., Kweon H.S., Lee Y.B. The crystallographic, magnetic properties of Al, Ti doped $CoFe_2O_4$ powders grown by sol–gel method *J. Magn. Magn. Mater.* **2004**, *283*, 103-108.
16. Virden A., Wells S., O'Grady K. Physical and magnetic properties of highly anisotropic cobalt ferrite particles *J. Magn. Magn. Mater.* **2007**, *316*, e768-e771.
17. Mahmoudi M., Sant S., Wang B., Laurent S., Sen T. Superparamagnetic iron oxide nanoparticles (SPIONs): development, surface modification and applications in chemotherapy *Adv. Drug Delivery Rev.* **2011**, *63*, 24-46.
18. Lu X., Liang G., Sun Q.,Yang C. High-frequency magnetic properties of Ni-Zn ferrite nanoparticles synthesized by a low temperature chemical method *Mater. Lett.* **2011**, *65*, 674-676.
19. Zheng H., Wang J., Lofland S. E., Ma Z., Mohaddes-Ardabili L., Zhao T., Salamanca-Riba L., Shinde S. R., Ogale S. B., Bai F., Viehland D., Jia Y., Schlom D. G., Wuttig M., Roytburd A., and Ramesh R. Multiferroic $BaTiO_3$-$CoFe_2O_4$ Nanostructures *Science* **2004**, *303*, 661-663.

20. Duong G. V. and Groessinger R. Effect of preparation conditions on magnetoelectric properties of CoFe$_2$O$_4$–BaTiO$_3$ magnetoelectric composites *J. Magn. Magn. Mater.* **2007**, *316*, e624-e627.

21. Raidongia K., Nag A., Sundaresan A., Rao C. N. R. Multiferroic and magnetoelectric properties of core-shell CoFe$_2$O$_4$@BaTiO$_3$ nanocomposites *Appl. Phys. Lett.* **2010**, *97*, 062904.

22. Lu X., Kim Y., Goetze S., Li X., Dong S., Werner P., Alexe M., Hesse D. Magnetoelectric Coupling in Ordered Arrays of Multilayered Heteroepitaxial BaTiO$_3$/CoFe$_2$O$_4$ Nanodots. *Nano Lett.* **2011**, *11*, 3202-3206.

23. Bauer M. J., Wen X., Tiwari P., Arnold D. P. and Andrew J. S. Magnetic field sensors using arrays of electrospun magnetoelectric Janus nanowires *Microsyst. Nanoeng.* **2018**, *4*, 37.

24. Erdem D., Bingham N. S., Heiligtag F. J., Pilet N., Warnicke P., Vaz C. A. F., Shi Y., Buzzi M., Rupp J. L. M., Heyderman L. J., and Niederberger M. Nanoparticle-Based Magnetoelectric BaTiO$_3$–CoFe$_2$O$_4$ Thin Film Heterostructures for Voltage Control of Magnetism *ACS Nano* **2016**, *10*, 9840-9851.

25. Cheng C., Dai J., Li Z. and Feng W.Preparation and magnetic properties of CoFe$_2$O$_4$ oriented fiber arrays by electrospinning *Materials* **2020**, *13*, 3860-3870.

26. Fallarino L., Quintana M., Rojo E. L. , and Berger A. Suppression of Coercivity in Nanoscale Graded Magnetic Materials *Phys. Rev. Appl.* **2021**, *16*, 034038(6).